AGU PUBLICATIONS

JGR

Journal of Geophysical Research: Solid Earth

RESEARCH ARTICLE

10.1002/2015JB012036

Key Points:
- Heat fluxes in drained, low-pressure subglacial eruption cavities are estimated
- Heat fluxes are lower than those inferred from recent volcanic eruptions

Supporting Information:
- Data Set S1 Caption
- Data Set S1

Correspondence to:
D. C. Woodcock,
d.woodcock@lancaster.ac.uk

Citation:
Woodcock, D. C., S. J. Lane, and J. S. Gilbert (2016), Ice-melt rates during volcanic eruptions within water-drained, low-pressure subglacial cavities, *J. Geophys. Res. Solid Earth*, *121*, 648–662, doi:10.1002/2015JB012036.

Received 14 MAR 2015
Accepted 24 JAN 2016
Accepted article online 27 JAN 2016
Published online 18 FEB 2016

Ice-melt rates during volcanic eruptions within water-drained, low-pressure subglacial cavities

D. C. Woodcock[1], S. J. Lane[1], and J. S. Gilbert[1]

[1]Lancaster Environment Centre, Lancaster University, Lancaster, UK

Abstract Subglacial volcanism generates proximal and distal hazards including large-scale flooding and increased levels of explosivity. Direct observation of subglacial volcanic processes is infeasible; therefore, we model heat transfer mechanisms during subglacial eruptions under conditions where cavities have become depressurized by connection to the atmosphere. We consider basaltic eruptions in a water-drained, low-pressure subglacial cavity, including the case when an eruption jet develops. Such drained cavities may develop on sloping terrain, where ice may be relatively shallow and where gravity drainage of meltwater will be promoted. We quantify, for the first time, the heat fluxes to the ice cavity surface that result from steam condensation during free convection at atmospheric pressure and from direct and indirect radiative heat transfer from an eruption jet. Our calculations indicate that the direct radiative heat flux from a lava fountain (a "dry" end-member eruption jet) to ice is c. 25 kW m^{-2} and is a minor component. The dominant heat transfer mechanism involves free convection of steam within the cavity; we estimate the resulting condensation heat flux to be c. 250 kW m^{-2}. Absorption of radiation from a lava fountain by steam enhances convection, but the increase in condensing heat flux is modest at c. 25 kW m^{-2}. Overall, heat fluxes to the ice cavity surface are likely to be no greater than c. 300 kW m^{-2}. These are comparable with heat fluxes obtained by single phase convection of water in a subglacial cavity but much less than those obtained by two-phase convection.

1. Introduction

Subglacial eruptions where magma has fragmented by explosion or granulation are often characterized by the rapid release of large quantities of meltwater and, on many occasions, by penetration of the overlying ice sheet or glacier ice to become subaerial [*Gudmundsson*, 2005]. Rapid release of meltwater has the potential to damage infrastructure in its path. In addition, the meltwater flow may mobilize volcanic sediments to generate lahars with potential for both infrastructure damage and loss of life [*Major and Newhall*, 1989].

We consider a subglacial fissure eruption in which a connection to the atmosphere becomes established and where two conditions are met: (1) meltwater drains from the cavity to allow the development of a vapor-dominated cavity; drainage will be promoted by steep terrain and/or large diameter meltwater conduits and (2) the cavity persists in the face of ductile ice flow that will tend to collapse the cavity; a condition favored by thin ice, cold (strong) ice and rapid melt back of the cavity walls. We discuss this second condition further in section 5.4. Under these conditions cavity pressure is low (i.e., near atmospheric); thus, explosive activity may be enhanced, and an eruption jet of pyroclasts with varying amounts of steam may develop in the subglacial cavity. *Magnússon et al.* [2012] describe the development of a minor eruption on slopes south of the summit caldera of Eyjafjallajökull, where the terrain was steeper and the ice thinner than at the summit region. Figure 4d in *Magnússon et al.* [2012] shows the appearance of a new cauldron that was not present in the corresponding image taken 38 s earlier. This earlier image shows a supraglacial meltwater channel starting some 300 m downslope from where the new cauldron later appears. A pair of images taken approximately an hour earlier shows no sign of this meltwater channel. *Magnússon et al.* [2012] suggest that the subglacial phase of this minor eruption was liquid dominated initially but subsequently drained meltwater.

For basaltic magmas, *Wilson et al.* [2013] proposed that a water-drained, low-pressure subglacial cavity may be produced if a subglacial sill, growing outward from a feeder dyke, reaches the edge of the enclosing ice body. Drainage of meltwater from the top of the sill is considered to be sufficiently rapid to allow the top of the sill to depressurize and undergo explosive fragmentation. Depressurization propagates backward toward the vent, initiating a Hawaiian-style lava fountain that "drills" through the overlying ice by pyroclast

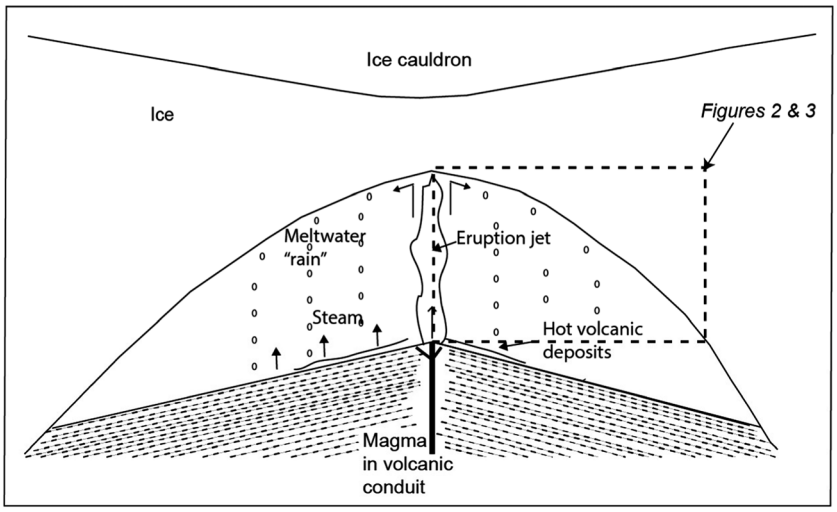

Figure 1. Schematic diagram of an ice cavity formed during a subglacial fissure eruption which has drained and depressurized to allow the formation of an eruption jet. In general, steam is produced by magma-water interaction within the volcanic conduit and by contact of the meltwater rain with hot volcanic deposits on either side of the eruption jet. The dashed rectangle indicates the location of Figures 2 and 3.

impact up to the unconstrained height of the fountain. Melting of the cavity then continues by radiative heat transfer from the lava fountain [*Wilson et al.,* 2013].

Figure 1 shows a schematic diagram of a water-drained, low-pressure ice cavity formed during a subglacial fissure eruption and containing an eruption jet. In this scenario, we expect the cavity fluid to be at or slightly above atmospheric pressure with the connection to the atmosphere maintained by the flow of hot meltwater or steam from the cavity to the edge of the enclosing ice body. The nature of the eruption jet will depend on the degree of magma-water interaction within the shallow volcanic conduit. For minimal interaction between water and basaltic magma a lava fountain may become established. As the extent of magma-water interaction increases, a lava fountain is progressively transformed to an ash-laden steam jet. This behavior is well illustrated around 5 min into a video clip of the 1959–1960 Kilauea eruption [*YouTube*, 2007], where the magma intermittently contacts shallow groundwater. The cavity fluid is expected to comprise mainly steam (water vapor), sourced from magmatic gas and phreatomagmatic activity. For the dry end-member case of a lava fountain we envisage that much of the phreatomagmatic steam is produced by contact of the meltwater rain from the cavity roof onto short clastogenic lava flows on either side of the lava fountain and by the interaction of hot spatter with water on the floor of the cavity. The spatter may fragment, cool rapidly, and generate copious amounts of steam. Any steam generated that is not condensed within the cavity may be vented out of the cavity. The presence of an eruption jet is, however, not necessary for heat transfer from magma to ice within the cavity. Hot lava or hot pyroclasts proximal to the vent will drive a free convective circulation that comprises an ascending limb of steam over the vent together with a descending limb of steam and water droplets adjacent to the cavity walls, where condensation of steam occurs. We show in section 3 that steam condensation is the primary heat transfer mechanism in water-drained low-pressure subglacial eruption cavities.

In this paper we quantify ice melt rates during volcanic eruptions within low-pressure subglacial drained cavities and compare the results with other subglacial eruption scenarios, specifically where the subglacial eruption cavity is filled with liquid water or steam at or near glaciostatic pressure [*Woodcock et al.,* 2014, 2015]. In particular, we consider (1) direct radiative transfer from the surface of pyroclasts in the outer envelope of an eruption jet to the walls and roof of the ice cavity, (2) steam condensation that occurs during free convection within the cavity, and (3) the possibility that convection may be enhanced by absorption of radiation from the jet by the steam in the cavity. In particular, we attempt, for the first time, to quantify heat transfer rates within an idealized model system using published heat transfer methods to estimate likely heat fluxes.

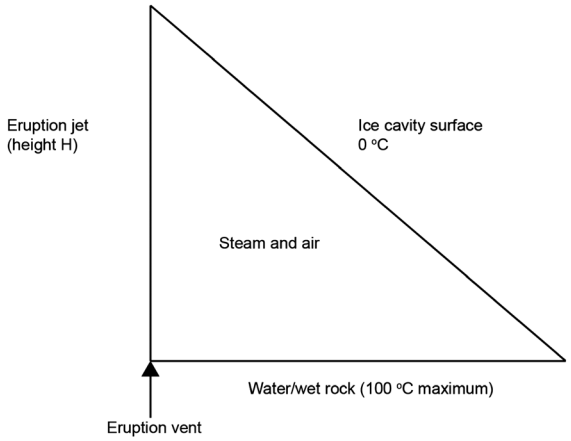

Figure 2. Conceptual model for radiative heat transfer from a linear, dyke-fed eruption jet in a subglacial cavity at atmospheric pressure. The cavity is assumed symmetrical about a center line above the eruption vent and the diagram shows the right hand side of the cavity only.

2. Direct Radiative Heat Transfer

In this section we estimate the heat transfer rate by direct radiative heat transfer between a linear dyke-fed eruption jet and an overlying ice cavity that is drained and vented to atmospheric pressure. We develop a first-order conceptual model of the system to estimate the heat flux on the ice cavity surface. We focus on lava fountains here because they are likely to have the highest radiative heat flux.

2.1. Conceptual Model

Figure 2 shows the conceptual model used for the radiation calculations. For expediency, we assume an ice cavity at atmospheric pressure that is triangular in cross section within which a lava fountain extends to the cavity roof. Both the cavity and the lava fountain extend along a linear eruption fissure that is long compared to the height of the cavity. We model the lava fountain as a vertical planar surface that radiates in all directions (i.e., as a "diffuse" or "Lambert" surface). The emissivity of lava approaches unity [*Pinkerton et al.,* 2002], so the lava fountain surface can be considered as a black body.

The assumption of a complete wall of lava (curtain of fire) without gaps overestimates the radiative heat flux but may be reasonable for the early stages of a Hawaiian-style fissure eruption. As the eruption progresses, activity often becomes localized to discrete locations along the vent [*Vergniolle and Mangan*, 2000]. For the analysis of this situation a model with axisymmetric symmetry may be more appropriate.

The direct radiative heat flux from the lava fountain has a strong dependence on the temperature of pyroclast surfaces that can "see" the ice surface. *Davies et al.* [2011] measured temperatures of up to 1140°C during thermal infrared (FLIR) observations of small (2–3 m high) lava fountains from the Erta' Ale lava lake, although this temperature must be regarded as an extreme case. For larger lava fountains the heat lost from pyroclasts by radiation and forced convection as pyroclasts travel through the fountain may be considerable; thus, FLIR-determined temperatures of lava fountains are generally much lower than those measured at Erta' Ale. For example, *Spampinato et al.* [2008] recorded lava fountain temperatures of around 700°C during the Etna 2002–2003 fissure eruption for fountains 100–300 m high erupting along a 1 km fissure. Within the "wet" environment of a subglacial cavity, lava fountain temperatures may be reduced further by magma-water interaction.

Although clear ice is transparent to visible radiation it is almost opaque to infrared radiation [*Brandl and Warren*, 1993]. Black body radiation at 700°C has a peak energy wavelength λ_{max} of around 3 μm, with more than 99% of the radiative energy at wavelengths longer than 1 μm [*Incropera and DeWitt*, 1996]. *Hobbs* [1974] tabulates data on the wavelength-dependent absorption coefficient for ice; these data show that most of the radiation emitted by the lava fountain will be absorbed in the first millimeter below the surface of the ice. Accordingly, we model the ice surface as a black body at 0°C.

The base of the cavity may comprise a layer of wet rock or pools of meltwater. The water will absorb radiation from the lava fountain but cannot attain a temperature greater than 100°C, the boiling point of water at 0.1 MPa. The cavity base will reradiate to the ice cavity, but the radiative flux will be small and is neglected.

The gas in the cavity will comprise a mixture of air and steam at atmospheric pressure. Dry air is almost transparent to infrared radiation, while steam absorbs infrared radiation to some degree. The presence of steam in the cavity will reduce the radiative flux from the lava fountain to the ice cavity because the steam will absorb some of the radiation from the lava fountain and reradiate it at a lower temperature. In section 2.2 we assume that there is no absorbing medium in the cavity and that the lava fountain surface can exchange radiation

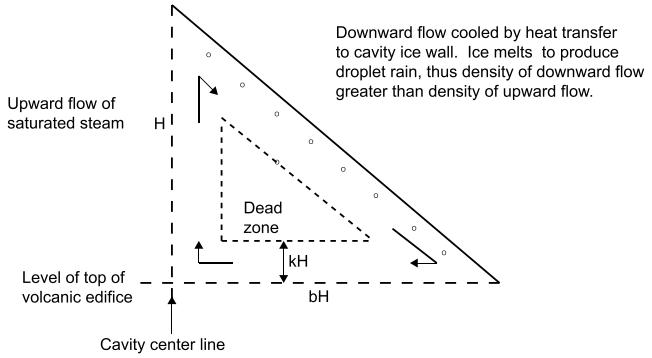

Figure 3. Free convective heat transfer and ice melting in a model subglacial eruption cavity. The cavity is symmetrical about the center line, and the right-hand half of the cavity only is shown. The third dimension (length) extends into the paper with the model developed for unit length.

directly with the ice cavity surface. The resulting heat flux is thus an upper bound on the likely radiative heat flux.

2.2. Radiative Heat Transfer Between Surfaces

In the absence of an absorbing medium in the cavity, radiation exchange between surfaces depends on the geometry and orientation of the surfaces as well as the radiation properties and temperatures of the surfaces. Geometry and orientation are accounted for by defining a "view factor," F_{ij}, which is the fraction of the radiation leaving surface i that is intercepted by surface j. In general, the evaluation of view factors is complex; however, Hottel's "crossed string" method [*Hottel and Sarofim,* 1967] can be used for surfaces that are long in one direction.

The net power radiated per unit length from one side of the lava fountain to one half of the ice surface (both considered to be black bodies) is given by *Incropera and DeWitt* [1996]:

$$E = \sigma AF\left(T_L^4 - T_i^4\right), \tag{1}$$

where σ is the Stefan-Boltzmann constant ($5.67\times10^{-8}\,\mathrm{W\,m^{-2}\,K^{-4}}$), A is the area of the lava fountain ($=H\,\mathrm{m^2\,m^{-1}}$), T_L and T_i are the lava and ice absolute temperatures, and F is the view factor of the ice surface from the lava fountain ($=1/\sqrt{2}$, see Appendix A). The surface of the ice exposed to radiation is $H\sqrt{2}\,\mathrm{m^2\,m^{-1}}$. The heat flux on the ice surface is thus given by

$$Q = \frac{\sigma\left(T_L^4 - T_i^4\right)}{2}. \tag{2}$$

For a lava fountain with a mean effective surface temperature of 700°C, the resulting heat flux is $25\,\mathrm{kW\,m^{-2}}$. Direct radiative heat fluxes thus appear to be much smaller than some of the heat fluxes calculated for convective heat transfer in both flooded and drained cavities [*Woodcock et al.,* 2014, 2015], where heat fluxes of up to $5\,\mathrm{MW\,m^{-2}}$ are plausible. We conclude that direct radiative heat transfer is likely to be a minor ice melting mechanism within drained, low-pressure subglacial eruption cavities.

3. Steam Condensation Heat Transfer From Free Convection

3.1. Introduction

In this section, we develop a model for the convection of saturated steam within a roofed cavity in the absence of an eruption jet. We consider the effect of an eruption jet on the convection in section 4. Condensation is the principal mechanism of heat transfer from the circulating steam to the sloping ice cavity roof. The heat flux may be evaluated using the method used in *Woodcock et al.* [2015], given a value for the convective circulation velocity.

The condensate and meltwater produced on the ice surface is envisaged to drip from the ice cavity roof in a rain of droplets. The presence of these droplets drives the circulation by density increase and by transferring momentum to the circulation.

3.2. Model Development

Figure 3 shows the elements of the model for the circulation within a prismatic cavity of triangular cross section with a height H and a basal half width bH. The triangular shape is chosen for expediency but the model could be generalized for other geometries. The circulation comprises an upward flow of steam parallel to the cavity center line, followed by a return downward flow along the sloping roof of the cavity (where heat transfer melts ice) followed by a horizontal flow to complete the loop. The flow is assumed to be confined to a

channel of width kH ($k < 0.5$) that is constant for the whole of the circulation. As a starting point, we assume a constant volume drained cavity, where melt rates are matched to ductile ice creep rates.

3.2.1. Driving Force for Circulation

The presence of the droplets in the downward flow increases the density and thus contributes to the pressure difference that drives convection. This "droplet density" ρ_{dr} is given by

$$\rho_{dr} = \frac{m_{cmw}}{u_t}, \tag{3}$$

where m_{cmw} is the flux of condensate and meltwater in the droplet rain and u_t is the average droplet terminal velocity (Appendix B). The resulting pressure difference is thus $\rho_{dr}\, gH$.

The motion of the droplets also contributes to the pressure difference that drives convection. As droplets fall, they experience a drag force that is equal to their weight. An equal and opposite force acts on the surrounding steam and this force has a component in the steam flow direction parallel to the cavity roof. The resulting effect, expressed as a pressure, is given by $\rho_{dr}\, gH$. The overall "driving" pressure difference is thus

$$\Delta P_{dr} = 2gH\rho_{dr}. \tag{4}$$

3.2.2. Overall Circulation Flow

The momentum balance over an element of the flow with height dh, density ρ, velocity u, and pressure P is

$$dP = \rho g dh + 0.5\rho u^2 dK + \rho u du, \tag{5}$$

where the three terms on the right hand side are the "gravitational," "frictional," and "accelerational" pressure changes, respectively, and dK is the loss coefficient [*Massey*, 1970].

For the circulation loop within the cavity the net pressure and velocity changes are zero and the mass flow rate per unit area ρu is constant. Thus, equation (5) can be integrated around the circulation loop to give

$$g\int \rho \; dh + 1/2\int \rho u^2 \; dK = 0. \tag{6}$$

The first term comprises the net pressure difference that drives the convective circulation flow. This driving pressure difference is balanced by the second term: the pressure loss due to friction and change of direction within the circulation loop. An expression for this "resisting" pressure difference ΔP_{res} can be developed by adapting the expression in *Woodcock et al.* [2014]; thus,

$$\Delta P_{res} = 0.5\left(\frac{m}{kH}\right)^2 \times \left(\frac{K_1}{\rho_1} + \frac{K_2}{\rho_2}\right), \tag{7}$$

where K_1 and K_2 are the loss coefficients for the bends in the circulation loop and ρ_1 and ρ_2 are the densities at the top and bottom of the upward flow, respectively.

The circulation flow rate can be determined by equating the driving and resisting pressure differences:

$$m = 2kH\left[\frac{gH\rho_{dr}}{K_1/\rho_1 + K_2/\rho_2}\right]^{0.5}. \tag{8}$$

The circulation velocity is used to update the value of the condensing heat flux and equation (8) is reevaluated to convergence. Fortunately, for the range of circulation velocities encountered, the heat flux is relatively insensitive to velocity, so satisfactory convergence can be obtained within one or two iterations.

3.3. Results

We evaluate equation (8) using the same conditions as the reference case in Table 1. The resulting mass flow rate per unit length of cavity is 13.5 kg s^{-1} m^{-1}; the corresponding condensing heat flux is 186 kW m^{-2}. There is thus significant heat transfer by free convection within the cavity, independent of the presence of an eruption jet.

4. Enhancement of Free Convection by Radiative Heat Transfer

4.1. Introduction

In this section we establish the extent to which the presence of an eruption jet enhances the circulation. We consider absorption of radiation by the steam adjacent to the eruption jet within a roofed cavity during a

Table 1. Sensitivity of Model Results to Changes in Input Variables (Names of Variables Changed and Value of Variable Changed Are in Italics)[a]

	Case							
Variable	Reference	2	3	4	5	6	7	8
Cavity height, H (m)	50	*100*	50	50	50	50	50	50
Cavity aspect ratio, b	2	2	*4*	2	2	2	2	2
Flow area fraction, k	0.05	0.05	0.05	*0.1*	0.05	0.05	0.05	0.05
Bend loss coefficients, K[b]	1	1	1	1	*2*	1	1	1
Jet temperature[c] (K)	973	973	973	973	973	*773*	*370*	973
Cavity fluid pressure (MPa)	0.1	0.1	0.1	0.1	0.1	0.1	0.1	*0.2*
Top[d] steam temperature (K)	394	389	395	385	403	380	370	405
Top steam velocity ($m\,s^{-1}$)	11.2	16.2	10.9	10.3	8.3	9.8	8.6	10.4
Circulation rate ($kg\,s^{-1}\,m^{-1}$)	16.5	48.3	16.0	31.1	12.0	15.0	13.5	30.0
Heat flux ($kW\,m^{-2}$)	211	243	209	203	204	199	186	315

[a]The noncondensable mole fraction is 0.1.
[b]Factor relative to reference case.
[c]Mean radiant temperature of pyroclast surfaces.
[d]Top of upward flow.

subglacial eruption. The consequent temperature increase and reduction in density as the steam is superheated will provide additional driving force and enhance the free convection. In section 4.2, we develop a model for this mechanism in order to estimate the likely melting heat flux.

Studies of free convection in vertical channels have been reported in the literature. *Cheng and Muller* [1998] and *Li et al.* [2013] carried out numerical studies of free convection of air in vertical channels where one plane wall was heated and the opposite wall was unheated apart from radiative heat transfer across the channel. In both studies the air was assumed to be radiatively transparent and any changes in air temperature to occur by convective heat transfer from the vertical walls. The situation considered by *Cheng and Muller* [1998] and *Li et al.* [2013] is not the situation that we envisage, where steam can absorb radiation. However, we are not aware of any study in which a freely convecting fluid is heated by absorption of thermal radiation.

The absorption of a collimated beam of monochromatic radiation may be modeled by the Beer-Lambert law [*Incropera and DeWitt,* 1996]:

$$dI = -\kappa I dz, \tag{9}$$

where dI is the amount of radiation absorbed from a beam with an incident radiative flux (I) over a thickness dz and κ is the attenuation coefficient. If κ is constant through a finite thickness L, equation (9) may be integrated to give

$$\left(\frac{I}{I_o}\right) = e^{-\kappa L}, \tag{10}$$

where I_o is the incident radiative flux on the gas layer of thickness L (known as the "beam length") and I is the flux emerging from the layer.

For absorption of radiation by a gas, equation (10) may be written as

$$\ln\left(\frac{I}{I_o}\right) = -\phi pL \tag{11}$$

where p is the partial pressure of the absorbing gas in the layer and ϕ is the absorption coefficient. The product pL is known as the optical depth. The absorption coefficient for a given waveband in general depends on temperature and total pressure.

A hot surface such as the surface of a lava fountain emits a continuous spectrum of radiation. In order to evaluate the total radiation absorbed by the gas one needs to evaluate the absorption for each increment of waveband and integrate over the whole spectrum. Hottel [*Hottel and Sarofim*, 1967] tackled this problem by considering the emission of radiation from an isothermal hemisphere of gas to a surface element at the center of its bounding diameter. Hottel defined a "standard emissivity" ε_g as the ratio of the radiation from the gas hemisphere to the radiation from a hemispherical black body shell with the same diameter and at the same temperature. Values of standard emissivities, which depend on the nature and optical depth of the absorbing gas, together with the gas temperature and total pressure, are summarized in *Hottel and Sarofim* [1967].

The values of standard emissivity relate to a hemispherical volume of gas. Hottel enabled his results to be extended to other geometries by his concept of "mean beam length" (L_e): the radius of a hemisphere of gas for which the emissivity is the same as the volume of gas under consideration [*Hottel and Sarofim,* 1967]. Tables of mean beam length for a number of geometries, together with Hottel's charts of standard emissivity, are widely used in the engineering solution of radiative heat transfer problems [*Hottel and Sarofim,* 1967; *Incropera and DeWitt,* 1996].

Finally, *Hottel and Sarofim* [1967] showed that the absorptivity α_g of a gas, at temperature T_g, that absorbs radiation from a black body with a surface at temperature T_s should be given by

$$\alpha_g = \varepsilon_g \left(\frac{T_g}{T_s}\right)^{0.5}, \tag{12}$$

where ε_g is the gas emissivity evaluated at T_s and for a modified mean beam length of L_e (T_s/T_g). In practice, an exponent on the temperature ratio of 0.45 provides a better fit to experimental data [*Incropera and DeWitt,* 1996].

4.2. Model Development

4.2.1. Upward Flow

Consider an element of unit length with a vertical thickness dh at height h above the base of the model cavity in the upward flow. We assume that any horizontal variation in steam temperature in an element is eliminated by turbulence; thus, the steam temperature can be defined by T_g (h). The net radiative heat transfer rate per unit length dq into the steam flow through this element is

$$\mathrm{d}q = \sigma\left(\alpha_g T_L^4 - 2\varepsilon_g T_g^4\right)\mathrm{d}h, \tag{13}$$

where σ is the Stefan-Boltzmann constant, T_L is the temperature of the lava fountain surface (assumed independent of h), and α_g and ε_g are the absorptivity and emissivity of the steam at height h. The factor of 2 arises because the steam flow emits radiation in both directions. The net radiative heat transfer raises the temperature of the steam by dT_g:

$$\mathrm{d}q = mC_p\mathrm{d}T_g, \tag{14}$$

where m is the steam mass flow rate per unit length with specific heat capacity C_p. Equations (13) and (14) may be combined to produce an equation for the rate of change of steam temperature with height within the upward flow:

$$\frac{\mathrm{d}T_g}{\mathrm{d}h} = \frac{\sigma\left(\alpha_g T_L^4 - \varepsilon_g T_g^4\right)}{mC_p}. \tag{15}$$

For steam at 0.1 MPa, emissivities are almost independent of temperature at long optical depths over the temperature range 373–900 K [*Incropera and DeWitt*, 1996]. The dependency of emissivity on optical depth pL can be represented by the equation

$$\varepsilon_g = 0.6 - 0.087 \ln\left(\frac{6.1}{pL}\right) \quad \text{with} \quad 0 \le \varepsilon_g \le 1, \tag{16}$$

where the mean beam length for this geometry is equal to 1.8 kH [*Incropera and DeWitt*, 1996]. The absorptivity for steam at 0.1 MPa is given by

$$\alpha_g = \varepsilon_g \left(\frac{T_g}{T_L}\right)^{0.45}, \tag{17}$$

where ε_g is evaluated at T_L for the modified optical depth of pL (T_L/T_g).

Equation (15) cannot be solved analytically but may be solved by numerical methods. The temperature rise ΔT_g over an element of finite vertical width ΔH is given by

$$\Delta T_g = \frac{\Delta H \sigma\left(\alpha_g T_L^4 - \varepsilon_g T_g^4\right)}{mC_p}. \tag{18}$$

The steam temperature, and thus the steam density, can be determined for each element for any circulation rate. The pressure difference over element i due to the weight of the steam with density ρ_i is

$$\Delta P_i = \rho_i g \Delta H. \tag{19}$$

The corresponding pressure difference for the whole upward flow is thus

$$\Delta P_r = g\,\Delta H\,\Sigma\rho_i. \tag{20}$$

The pressure difference between the top and base of the cavity is of order 10^3 Pa compared with the total pressure of 10^5 Pa; density differences due to changes in pressure may thus be neglected.

4.2.2. Downward Flow

Within the downward flow, the principal mechanism for heat transfer from the circulating steam to the ice surface is condensation. The passage of condensate and meltwater droplets through the vertical width of the downward flow cools the circulating steam further by convection and radiation to the droplet surfaces (Appendix B). In addition, heat is transferred from the hot steam to the ice surface by radiation, although this is only significant at high steam temperatures.

If the total heat removal rate per unit length is Δq for an element ΔH of the downward flow, the corresponding temperature decrease ΔT_g is given by

$$\Delta T_g = \frac{\Delta q}{mC_p}. \tag{21}$$

Equation (21) is valid provided that the steam temperature is greater than the local boiling point; below the saturation level in the downward flow the temperature is then constant. The steam density for each element can then be evaluated once the various contributions to Δq have been calculated.

The pressure difference for the downward flow is thus

$$\Delta P_d = g\Delta H(\Sigma\rho_i + \Sigma\rho_{\mathrm{dr}}), \tag{22}$$

where ρ_i comprises the sum of the steam density and the droplet density (section 3.2.1). The net pressure difference that drives the convective circulation flow is given by

$$\Delta P_{dr} = \Delta P_d - \Delta P_r. \tag{23}$$

This driving pressure difference is balanced by the pressure loss due to friction and change of direction within the circulation loop. An expression for this resisting pressure difference ΔP_{res} is given by equation (7) in section 3.2.2.

The equations that describe the fluid flow and heat transfer have been set up as a spreadsheet in Excel. The circulation flow rate that occurs when the driving and resisting pressure differences are equal can be found using the Goal Seek option. The resulting circulation velocities and temperatures are used to determine the heat flux from steam condensation; thus, both the circulation flow model and the steam condensation model need to be converged simultaneously.

4.3. Results

Table 1 shows the results of a "reference case" calculation, together with a number of sensitivity studies to illustrate the effect of varying cavity height, aspect ratio, flow width, and loss coefficients together with the effect of changing eruption jet surface temperature and cavity pressure. Case 7, with an eruption jet surface temperature set to 370 K, has results that are identical to those calculated in section 3.3 for free convection of steam in the absence of an eruption jet.

Our mechanism requires the generation of steam as well as radiative heat from the eruption jet. Steam generation will require some degree of phreatomagmatic interaction within the shallow volcanic conduit or in the cavity, although the degree of interaction may vary significantly in time and space. Figure 1 shows the case where steam production occurs on either side of the eruption jet by contact of the "rain" of condensate from the roof onto hot volcanic deposits. For the reference case we have chosen a temperature of 973 K for the eruption jet surface temperature. Increasing degrees of phreatomagmatic interaction will result in a colder eruption jet: we explore this with a "step out" case in Table 1.

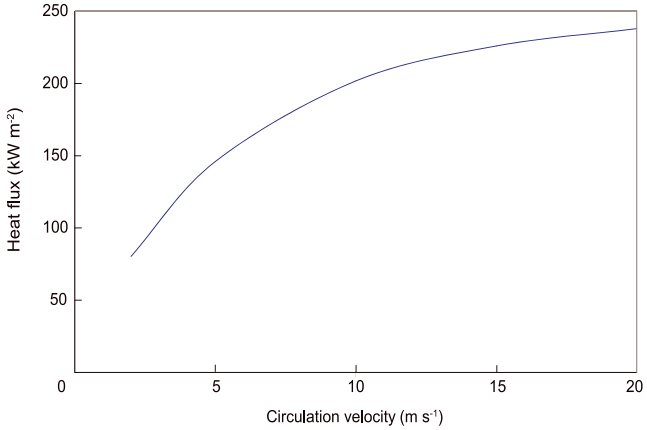

Figure 4. Variation of condensing heat flux with circulation velocity for a subglacial cavity at 0.1 MPa, with condensation from saturated vapor at 373 K. For the range of velocities encountered on Table 1 the heat flux varies by approximately 20%.

Three general conclusions can be drawn from the results presented in Table 1. First, steam temperatures are relatively low, precluding significant heat transfer by radiation from the steam. Thus, in the downward flow, heat transfer is dominated by condensation. Second, the circulation velocities are sufficiently fast that heat flux is relatively insensitive to velocity (Figure 4). Third, for the same conditions, the radiative enhancement of heat flux (an additional 25 kW m^{-2} for the reference case conditions) is relatively modest. All heat fluxes are much smaller than heat fluxes calculated for convective heat transfer in both flooded and drained cavities [*Woodcock et al.,* 2014, 2015]. The effect of individual variables is discussed below.

Variation in Cavity Height H (*Compare Case 2 With Reference Case*). Doubling cavity height potentially doubles the driving ΔP, while the resisting ΔP is proportional to $(m/kH)^2$ via equation (7). Thus, circulation rate m might be expected to increase by $2^{3/2}$ or 2.8; this is close to the determined increase.

Variation in Cavity Aspect Ratio b (*Compare Case 3 With Reference Case*). Increasing aspect ratio should increase circulation rate because desuperheating of the downward flow is completed at a greater height, so the driving force for circulation is increased. The effect is small because the length of cavity wall needed for desuperheating is short and most of the downward flow comprises saturated steam.

Variation in Flow Width (*Compare Case 4 With Reference Case*). Circulation rate is expected to increase linearly with flow width (at constant H). The observed increase is slightly less because the temperature increase in the upward flow decreases slightly, thus reducing the driving force for circulation.

Variation in Bend K Value (*Compare Case 5 With Reference Case*). Doubling the K values should reduce the circulation rate by a factor of $2^{1/2}$. However, a reduced circulation rate allows a larger temperature rise in the upward flow, slightly increasing the driving force for circulation.

Variation in Eruption Jet Temperature (*Compare Case 6 and 7 With Reference Case*). Changes in eruption jet temperature appear to have little effect on heat flux. There are two reasons for this. First, provided that the circulation velocity is sufficiently fast, the condensing heat flux is relatively insensitive to velocity. Second, the circulation has two drivers. One driver is the density difference produced by the temperature difference between the upward and downward flows—this depends on the amount of radiation absorbed by the upward flow, which in turn depends on the temperature of the eruption jet. The second driver is the presence of liquid droplets in the downward flow—this increases the density difference between the upward and downward flow and transfers momentum into the downward flow (section 3.2.1). This second driver is largely independent of eruption jet temperature; it depends only on sufficient steam being available and the convection being "focused" with the upflow over the vent and downflow along the ice cavity walls.

Variation in Cavity Pressure (*Compare Case 8 With Reference Case*). Doubling the cavity pressure increases steam absorptivity by around 20% [*Incropera and DeWitt,* 1996] and doubles the density for a given temperature. The net effect is that the temperature rise in the upward flow is almost unchanged. In the downward flow, droplet density is increased due to reduced terminal velocity: this increases the driving force for circulation. The net effect is to increase the overall driving force for circulation by $2^{1/2}$, but this is balanced by a frictional pressure drop that is inversely proportional to steam density via equation (7). The resulting circulation rate is thus expected to increase by a factor of around $2^{3/4}$ (1.7), similar to the observed increase.

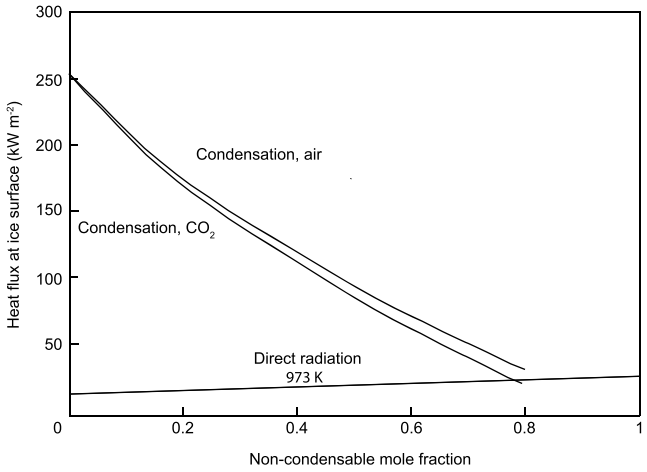

Figure 5. Variation of heat flux on the ice cavity surface with mole fraction and nature of the noncondensable component. Two curves are shown for the condensation heat flux during radiatively enhanced free convection for an eruption jet temperature of 973 K: one for air (which is assumed to be radiatively transparent) and one for CO_2 (with radiative properties of steam). A third solid line shows schematically the likely variation in direct radiative heat flux at 973 K. The total heat flux is the sum of the condensation and direct radiative heat fluxes.

5. Discussion

5.1. Concentration of Noncondensable Gases in the Cavity

The condensation heat flux depends on the concentration of noncondensable gases in the cavity. The reference case value of 0.1 mole fraction is justified as follows. The sources of noncondensable gases in a subglacial eruption cavity were reviewed by *Woodcock et al.* [2015]. They include air from melted ice (c. 0.5 kg/tonne magma) and the noncondensable gases, principally CO_2, exsolved from magma. The total magmatic gas exsolved is around 10 kg/tonne magma, of which c. 15% is noncondensable. The cavity is an open system that is vented at atmospheric pressure: the noncondensable gas concentration would thus be (0.5 + 1.5)/10.5 or 0.19 mass fraction (equivalent to 0.14 mole fraction). The rate of steam generation from magma-water interaction, together with magmatic steam, is likely to be in excess of the steam condensation rate. The excess steam will thus dilute the noncondensable gases.

We explore the sensitivity to noncondensable gas mole fraction for the reference case cavity pressure and dimensions. Figure 5 shows two curves for condensation heat flux versus noncondensable mole fraction: one curve assumes that the noncondensable component is air and the other assumes it to be CO_2, but with its radiative properties modeled by steam for expediency. The principal effect of increasing the noncondensable mole fraction is to reduce the condensation heat flux, as demonstrated in *Woodcock et al.* [2015]. Additional minor effects that arise from the nature of the noncondensable component are changes in gas density, gas absorptivity, and gas specific heat capacity. If the noncondensable component is radiatively transparent, then the absorptivity of the gas mixture in the upward flow decreases with increase in noncondensable mole fraction.

For comparison, Figure 5 also includes the direct radiation heat flux evaluated in section 2.2. The zero-steam value of 25 kW m^{-2} assumes that the cavity gases are radiatively transparent. As the proportion of steam increases, the direct radiation heat flux decreases because some of the radiation from the eruption jet is absorbed by the steam and reradiated at a cooler temperature. In the reference case, the absorptivity of the cavity gases is c. 0.3; a lower bound on the direct radiation flux is thus 25(1 − 0.3), i.e., c. 18 kW m^{-2}.

5.2. Liquid Film Thinning by Gas Shear

The condensing heat fluxes reported in section 4.3 neglect any effects due to thinning of the liquid film of meltwater and condensate by the cocurrent flow of steam. The effect of tangential shear on the liquid film thickness and thus on the condensing heat flux was studied by *Rohsenow et al.* [1956]. They showed that, for laminar films, the "no-shear" heat transfer coefficient should be increased by a factor of $[1 + (4U\tau_g/3g\sin\theta\rho_w k_l)]$, where τ_g is the tangential shear stress at the liquid film surface, U is the film heat transfer coefficient, θ is the inclination of the surface from the horizontal, and k_l is the liquid thermal conductivity. The ratio k_l/U may be replaced by the film thickness δ, whence the factor becomes $[1 + (4\tau_g/3g\sin\theta\delta\rho_w)]$, where the second term is approximately the ratio of the shear force to the gravitational force on the liquid film [*Rohsenow et al.,* 1956].

Rohsenow et al. [1956] extended their analysis to include turbulent liquid films and provided a method for evaluating τ_g. Application of their results to the reference case in Table 1 shows that tangential shear increases the heat flux by around 30%.

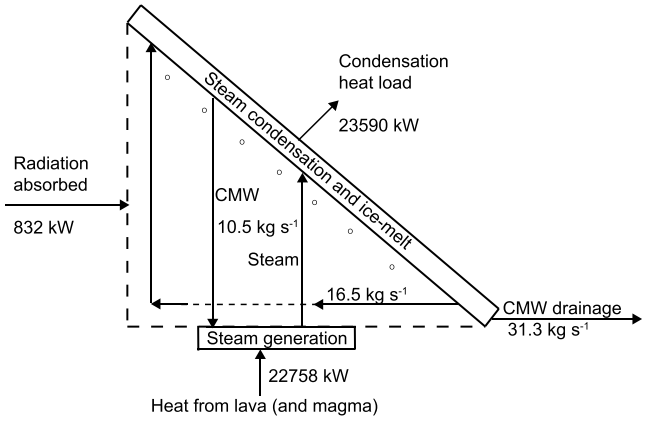

Figure 6. Block diagram of the overall mass and heat balance for the convection system within the ice cavity for the reference case in Table 1. Flow rates are for unit length of fissure. CMW = condensate plus meltwater.

5.3. Comparison With Inferred Fluxes From Recent Eruptions

In section 2 we showed that an upper bound on direct radiative heat flux is approximately 25 kW m^{-2}. Table 1 indicates condensing heat fluxes from radiatively enhanced free convection of 200–300 kW m^{-2}; these should be increased by 30% to account for tangential shear. Figure 4 indicates that any forcing of the convection by momentum transfer from the eruption jet is unlikely to increase heat fluxes significantly. Overall, heat fluxes from lava to ice cavity surface are likely to be no greater than 300–400 kW m^{-2}. These are similar to those calculated by *Woodcock et al.* [2014] for single phase convection in liquid-filled cavities.

Heat fluxes of 300–400 kW m^{-2} will melt ice with a vertical penetration rate of around 3–5 m h^{-1} if meltwater leaves the ice cavity surface at 0°C. The assumption of meltwater at 0°C is unrealistic but provides an upper bound on penetration rate. The rate is approximately halved for a meltwater temperature approaching the boiling point. These ice penetration rates may be compared with rates of 16 and 50 m h^{-1} inferred for the Gjálp 1996 eruption [*Gudmundsson et al.,* 2004] and the 2010 Eyjafjallajökull summit caldera eruption [*Magnússon et al.,* 2012], respectively. In both of these cases much of the evidence suggests that the subglacial cavities were predominantly liquid water filled.

5.4. The Effect of Ductile Ice Flow

In section 1 we mentioned that an eruption jet can only occur during subglacial eruptions if a cavity can persist in the face of ductile ice flow that will tend to collapse the cavity. *Tuffen* [2007] indicates that for a hemicylindrical cavity, the relative rate of cavity closure by ductile ice deformation is given by

$$\frac{1}{R}\frac{\mathrm{d}R}{\mathrm{d}t} = (\Delta P_a / nB)^n, \tag{24}$$

where R is the cavity radius, ΔP_a is the cavity under pressure (glaciostatic pressure in our case), B is the ice deformation parameter (a measure of ice strength), and n has a value of 3.

For a given ice thickness, a cavity developed in ice of a given strength can only be sustained in the face of ductile collapse if the melt back rate is sufficiently high. *Tuffen* [2007] explores this behavior and shows that explosive magmatism can only be sustained, for the Gjálp 1996 eruption rate, for cavity under pressures below 4 MPa (i.e., $<$ 400 m ice) in ice at 0° C. In section 5.3 we show that melt back rates are much lower than those inferred for the Gjálp 1996 eruption. This example illustrates that thin ice is a necessary condition for explosive activity within drained, low-pressure subglacial cavities in temperate glaciers.

5.5. Overall Mass and Heat Balance

Figure 6 shows the overall mass and heat balance for the convection system within the ice cavity for the reference case in Table 1. Of the 16.5 kg s^{-1} steam circulation per meter length of fissure, 10.5 kg s^{-1} m^{-1} condenses on the ice cavity roof, liberating heat at a rate of 23590 kW m^{-1} and producing 31.3 kg s^{-1} m^{-1} meltwater (at 370 K). The steam condensed is replenished by the evaporation of 10.5 kg s^{-1} m^{-1} condensate and meltwater (CMW); the remaining CMW drains from the cavity. Note that although the flows of condensing steam and the resulting condensate are shown as discrete arrows on the diagram, in reality they are diffuse flows that occur along the width of the cavity.

The radiant heat flux from the eruption jet at 700°C is 2541 kW m^{-1}. The radiation heat flow of 832 kW m^{-1} in Figure 6 is the radiation absorbed by the steam circulation from the eruption jet. The remaining radiation (1709 kW m^{-1}) is absorbed by steam in the rest of the cavity, by the ice roof and by the cavity floor.

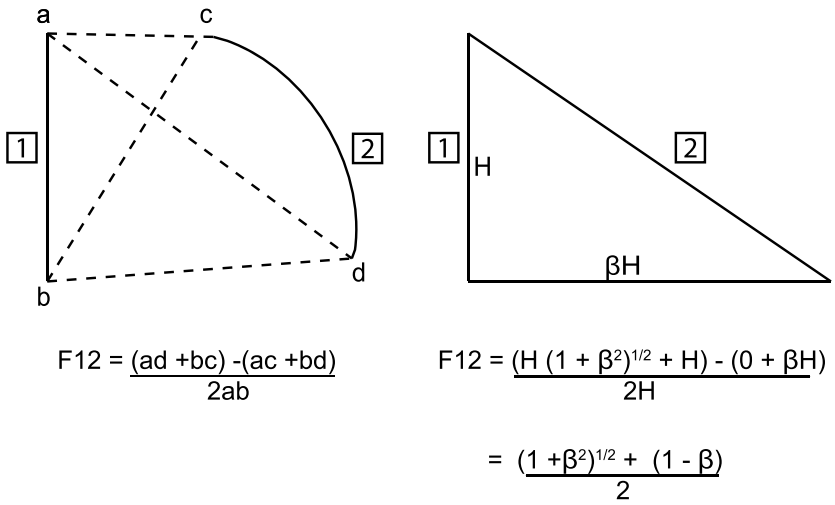

Figure A1. The diagram on the left-hand side shows the general version of Hottel's crossed string rule [*Hottel and Sarofim*, 1967], in which notional strings are attached to the ends of the two surfaces (labeled 1 and 2) as shown by the dashed lines. The formula for the view factor involves the difference between the sum of the crossed strings and the sum of the uncrossed strings. The diagram on the right-hand side applies the rule to the geometry of the subglacial cavity (with height *H*). If $\beta = 1$, the value of F_{12} is $1/\sqrt{2}$.

Ultimately, this radiation generates an additional 2.3 kg s^{-1} m^{-1} of meltwater that is not included within the mass flow rates in Figure 6.

The heat flow rates on Figure 6 demonstrate that much of the heat required for ice melt is provided by the latent heat of steam generated within the ice cavity. Radiative heat loss from the falling pyroclasts in the eruption jet is a small proportion of their initial heat content; thus, much of the initial heat content of the pyroclasts is retained on landing. We envisage efficient steam generation by the contact of hot pyroclasts with meltwater rain from the ice cavity roof and with the wet floor of the cavity.

6. Conclusions

We have used published heat transfer calculation methods to estimate heat fluxes to an ice cavity surface during subglacial fissure eruptions where shallow ice and steep terrain promote gravity drainage of meltwater and allow the cavity to depressurize. The principal conclusions are as follows.

1. Free convection can develop in the cavity with an ascending limb of steam over the vent together with a descending limb of steam and water droplets adjacent to the cavity walls, where condensation of steam occurs. The heat flux from steam condensation during free convection at atmospheric pressure is c. 250 kW m^{-2} when the effect of tangential shear on the liquid film is included.
2. For basaltic magmas, a subglacial lava fountain may develop. The direct radiative heat flux from lava fountain to ice cavity surface is c. 25 kW m^{-2}. Absorption of radiation by steam enhances the convective circulation but the increase in condensing heat flux is modest at c. 25 kW m^{-2}. The effects of radiation are thus minor compared to free convection.
3. Overall heat fluxes within water-drained, atmospheric pressure cavities during subglacial fissure eruptions are likely to be no greater than c. 300 kW m^{-2}. These are similar to those calculated by *Woodcock et al.* [2014] for single phase convection in liquid-filled cavities but much less than those obtained by two-phase convection within a liquid-dominated cavity.

Appendix A: Hottel's Crossed String Method

In general, the evaluation of view factors is complex; however, Hottel's crossed string method [*Hottel and Sarofim,* 1967] can be used for surfaces that are long in one direction. Figure A1 shows the general rule (on the left-hand side) and applies it to the geometry of the subglacial cavity (with height *H*) on the right hand side.

Appendix B: Heat Transfer to Droplets in the Downward Flow

The surface area available for heat transfer to droplets is given by

$$A_d = \frac{6\rho_{dr} kH}{d\rho_w}, \tag{B1}$$

where ρ_{dr} is the droplet density defined in equation (3), kH is the width of the circulation path, ρ_w and d are the density of liquid water and the droplet diameter, respectively. A_d is the droplet area per unit area of ice surface.

In turbulent flow, the terminal velocity u_t of a droplet with diameter d falling through steam with density ρ_i is given by

$$u_t = \left(\frac{4\rho_w g\mathrm{d}}{3\rho_i C_D}\right)^{1/2}, \tag{B2}$$

where C_D is the droplet drag coefficient and g is the gravitational acceleration.

The convective heat transfer coefficient (U) to the droplet surface may be calculated from the Ranz and Marshall correlation [*Ranz and Marshall*, 1952]

$$Nu = 2 + 0.6\ Re^{1/2} Pr^{1/3}, \tag{B3}$$

where Nu is the Nusselt number ($Nu = U\,d/k_g$), Re is the Reynolds number ($Re = u_t \rho_i\, d/\mu$), Pr is the Prandtl number ($Pr = \mu\, C_p/k_g$), and μ, C_p, and k_g are the viscosity, specific heat capacity, and thermal conductivity of steam, respectively.

Heat transfer by radiation to a droplet surface may be approximated by

$$Q_r = \sigma\left(\varepsilon_g {T_g}^4 - {T_d}^4\right), \tag{B4}$$

where Q_r is the net radiation (W per m^2 droplet area) and T_d is the droplet surface temperature (assumed to be the boiling point).

Notation

A	area of eruption jet per unit length, m.
B	ice deformation parameter, Pa $s^{-1/3}$.
A_d	heat transfer area of droplets per unit area of ice surface, dimensionless.
b	aspect ratio of cavity (ratio of basal half width to cavity height), dimensionless.
C_D	droplet drag coefficient, dimensionless.
C_p	specific heat capacity of steam, J kg^{-1} K^{-1}.
d	droplet diameter, m.
dh	increment of vertical height in cavity, m.
dI	amount of radiation absorbed from a beam of radiation, W m^{-2}.
dq	net radiative heat transfer rate into the steam flow, W.
dT_g	change in steam temperature, K.
dz	increment of thickness of absorbing medium, m.
E	net power radiated per unit length of eruption jet, W m^{-1}.
F	view factor, dimensionless.
g	gravitational acceleration, m s^{-2}.
H	height of subglacial cavity, m.
I	radiative flux emerging from a gas layer of thickness L, W m^{-2}.
I_o	incident radiative flux on a gas layer of thickness L, W m^{-2}.
k	ratio of channel width to cavity height, dimensionless.
k_g	thermal conductivity of steam, W m^{-1} K^{-1}.
k_l	thermal conductivity of liquid, W m^{-1} K^{-1}.
K	loss coefficient for overall circulation, dimensionless.
K_1	loss coefficient for top bend in the circulation loop, dimensionless.
K_2	loss coefficient for bottom bends in the circulation loop, dimensionless.

L	finite thickness of absorbing medium, m.
L_e	mean beam length, m.
m	steam mass flow rate per unit length, kg s^{-1} m^{-1}.
m_{cmw}	flux of condensate and meltwater in the droplet rain, kg s^{-1} m^{-2}.
Nu	Nusselt number ($Nu = U\,d/k$), dimensionless.
n	exponent in ice deformation equation (equation (24)), dimensionless.
P	pressure, Pa.
p	partial pressure of the absorbing gas in the layer, Pa.
pL	optical depth, Pa m.
Pr	Prandtl number ($Pr = \mu\, C_p/k$), dimensionless.
Q	heat flux to ice surface, W m^{-2}.
Q_r	net radiation to droplet surface, W m^{-2}.
q	heat transfer rate per unit length, W m^{-1}.
R	cavity radius, m.
Re	Reynolds number ($Re = u_t \rho_g\, d/\mu$), dimensionless.
T_d	droplet surface temperature, K.
T_g	gas temperature, K.
T_i	ice temperature, K.
T_L	temperature of eruption jet surface, K.
T_s	temperature of radiating surface, K.
U	heat transfer coefficient, W m^{-2} K^{-1}.
u	velocity, m s^{-1}.
u_t	average droplet terminal velocity, m s^{-1}.
α_g	absorptivity of a gas, dimensionless.
ΔH	vertical height of finite element, m.
ΔP	pressure difference, Pa.
ΔP_a	cavity underpressure, Pa.
ΔP_d	pressure difference for downward flow, Pa.
ΔP_i	pressure difference over vertical element, Pa.
ΔP_{dr}	driving pressure difference, Pa.
ΔP_r	pressure difference in upward flow, Pa.
ΔP_{res}	resisting pressure difference, Pa.
Δq	total heat removal rate per unit length for an element, W m^{-1}.
ΔT_g	temperature change of steam, K.
δ	liquid film thickness, m.
ε_g	gas emissivity, dimensionless.
κ	attenuation coefficient, m^{-1}.
μ	viscosity of steam, Pa s.
ϕ	absorption coefficient, Pa^{-1} m^{-1}.
ρ	density, kg m^{-3}.
ρ_{dr}	droplet density, kg m^{-3}.
ρ_i	steam density, kg m^{-3}.
ρ_w	liquid water density, kg m^{-3}.
ρ_1	density at top of upward flow, kg m^{-3}.
ρ_2	density at bottom of upward flow, kg m^{-3}.
σ	Stefan-Boltzmann constant, W m^{-2} K^{-4}.
τ_g	shear stress on liquid film surface, Pa.
θ	inclination of surface from horizontal, degree.

Acknowledgments
The data supporting this paper are available as supporting information. We sincerely thank Magnus Tumi Gudmundsson, John Stevenson, and an anonymous reviewer for their detailed comments during the review which have greatly improved the paper. We also thank the Editor André Revil and the Associate Editor for their comments. We are grateful to Lionel Wilson for his comments on an early version of this paper.

References

Brandl, R. E., and S. G. Warren (1993), Solar-heating rates and temperature profiles in Antarctic snow and ice, *J. Glaciol.*, *39*, 99–110.
Cheng, X., and U. Muller (1998), Turbulent natural convection coupled with thermal radiation in large vertical channels with asymmetric heating, *Int. J. Heat Mass Transfer*, *41*, 1681–1692.

Davies, G. D., L. Keszthelyi, and A. S. McEwen (2011), Estimating eruption temperature from thermal emission spectra of lava fountain activity in the Erta'Ale (Ethiopia) volcano lava lake: Implications for observing Io's volcanoes, *Geophys. Res. Lett.*, *38*, L21308, doi:10.1029/2011GL049418.

Gudmundsson, M. T. (2005), Subglacial volcanic activity in Iceland, in *Iceland: Modern Processes, Past Environments, Developments in Quaternary Science*, vol. 5, edited by C. J. Caseldine et al., pp. 127–151, Elsevier, Amsterdam.

Gudmundsson, M. T., F. Sigmundsson, H. Bjornsson, and T. Hognadottir (2004), The 1996 eruption at Gjálp, Vatnajökull ice cap, Iceland: Efficiency of heat transfer, ice deformation and subglacial water pressure, *Bull. Volcanol.*, *66*, 46–65.

Hobbs, P. V. (1974), *Ice Physics*, Clarendon, Oxford, U. K.

Hottel, H. C., and A. F. Sarofim (1967), *Radiative Heat Transfer*, McGraw Hill, New York.

Incropera, F. P., and D. P. DeWitt (1996), *Introduction to Heat Transfer*, John Wiley, New York.

Li, R., M. Bousetta, E. Chenier, and G. Lauriat (2013), Effect of surface radiation on natural convective flows and the onset of flow reversal in asymmetrically heated vertical channels, *Int. J. Therm. Sci.*, *65*, 9–27.

Magnússon, E., M. T. Gudmundsson, G. Sigurdsson, M. J. Roberts, F. Höskuldsson, and B. Oddsson (2012), Ice-volcano interactions during the 2010 Eyjafjallajökull eruption, as revealed by airborne radar, *J. Geophys. Res.*, *117*, B07405, doi:10.1029/2012JB009250.

Major, J. J., and C. G. Newhall (1989), Snow and ice perturbation during historical volcanic eruptions and the formation of lahars and floods, *Bull. Volcanol.*, *52*, 1–27.

Massey, B. S. (1970), *Mechanics of Fluids*, Van Nostrand Reinhold, London.

Pinkerton, H., M. James, and A. Jones (2002), Surface temperature measurements of active lava flows on Kilauea volcano, Hawaii, *J. Volcanol. Geotherm. Res.*, *113*, 159–176.

Ranz, W. E., and W. R. Marshall (1952), Evaporation from drops, *Chem. Eng. Prog.*, *48*, 141–146.

Rohsenow, W. M., J. H. Webber, and A. T. Ling (1956), Effect of vapor velocity on laminar and turbulent film condensation, *Trans. ASME*, *78*, 1637–1643.

Spampinato, L., S. Calvari, C. Oppenheimer, and L. Lodato (2008), Shallow magma transport for the 2002-3 Mt. Etna eruption inferred from thermal infrared surveys, *J. Volcanol. Geotherm. Res.*, *177*, 301–312.

Tuffen, H. (2007), Models of ice melting and edifice growth at the onset of subglacial basaltic eruptions, *J. Geophys. Res.*, *112*, B03203, doi:10.1029/2006JB004523.

Vergniolle, S., and M. Mangan (2000), Hawaiian and strombolian eruptions, in *Encyclopaedia of Volcanoes*, edited by H. Sigurdsson, pp. 447–461, Academic, San Diego, Calif.

Wilson, L., J. L. Smellie, and J. W. Head (2013), Volcano-ice interactions, in *Modelling Volcanic Processes*, edited by S. A. Fagents et al., pp. 275–299, Cambridge Univ. Press, Cambridge, U. K.

Woodcock, D. C., S. J. Lane, and J. S. Gilbert (2014), Ice-melt rates in liquid-filled cavities during explosive subglacial eruptions, *J. Geophys. Res. Solid Earth*, *119*, 1803–1817, doi:10.1002/2013JB010617.

Woodcock, D. C., J. S. Gilbert, and S. J. Lane (2015), Ice-melt rates by steam condensation during explosive subglacial eruptions, *J. Geophys. Res. Solid Earth*, *120*, 864–878, doi:10.1002/2014JB011619.

YouTube (2007), The Eruption of Kilauea 1959–1960, chap. 3, YouTube. [Available at https://www.youtube.com/watch?v=aa8Wr6xZPYI, accessed 14 January 2016.]